JACS
JOURNAL OF THE AMERICAN CHEMICAL SOCIETY
Article
pubs.acs.org/JACS

Drug-Induced Conformational and Dynamical Changes of the S31N Mutant of the Influenza M2 Proton Channel Investigated by Solid-State NMR

Jonathan K. Williams, Daniel Tietze, Jun Wang, Yibing Wu, William F. DeGrado, and Mei Hong*

Department of Chemistry, Iowa State University, Ames, Iowa 50011, United States

Department of Pharmaceutical Chemistry, University of California San Francisco, San Francisco, California 94158-9001, United States

Supporting Information

ABSTRACT: The M2 protein of influenza A viruses forms a tetrameric proton channel that is targeted by the amantadine class of antiviral drugs. A S31N mutation in the transmembrane (TM) domain of the protein has caused widespread amantadine resistance in most of the currently circulating flu viruses. Recently, a new family of compounds based on amantadine- and aryl-substituted isoxazole were discovered to inhibit the S31N channel activity and reduce replication of S31N-harboring viruses. We now use solid-state NMR spectroscopy to investigate the effects of one of these isoxazole compounds, WJ352, on the conformation of the S31N TM segment and the dynamics of the proton-selective residue, His37. Chemical shift perturbations show that WJ352 changes the conformational equilibrium of multiple TM residues, with the maximal perturbation occurring at the crucial Asn31. $^{13}C-^{2}H$ distance measurements and $^{1}H-^{1}H$ NOE cross peaks indicate that the adamantane moiety of the drug is bound in the spacious pore between Asn31 and Gly34 while the phenyl tail is located near Val27. Thus, the polar amine points to the channel exterior rather than to His37, in contrast to amantadine and rimantadine in the wild-type channel, suggesting that the drug is significantly stabilized by hydrophobic interactions between the adamantane and the TM peptide. ^{15}N and ^{13}C chemical shifts indicate that at low pH, His37 undergoes fast exchange among the τ tautomer, the π tautomer, and the cationic state due to proton transfer with water. The exchange rate is higher than the wild-type channel, consistent with the larger single-channel conductance of the mutant. Drug binding at acidic pH largely suppresses this exchange, reverting the histidines to a similar charge distribution as that of the high-pH closed state.

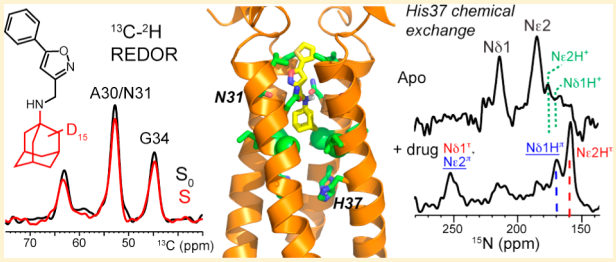

INTRODUCTION

The M2 protein of influenza A viruses spans the viral envelope and forms a tetrameric channel that conducts protons across the membrane when the external environment is acidic. This proton channel activity is important for virus uncoating[1,2] and in some viruses, also for maintaining the high pH of the trans-Golgi network to prevent premature conformational changes of hemagglutinin.[3] A single histidine residue, His37, in the transmembrane (TM) domain of the protein is responsible for pH activation and proton selectivity of the channel.[4] Detailed information about how His37 mediates proton conduction has been obtained from solid-state NMR studies of phospholipid-bound M2 TM peptides (M2TM).[5] At acidic pH, the imidazolium rings undergo small-amplitude reorientations[6] and exchange protons with water molecules at a rate of 10^5 s^{-1}.[7,8] The energy barrier of the ring motion, found to be at least 60 kJ/mol, is consistent with the proton-conduction energy barrier of ~100 kJ/mol measured in liposome assays.[9] ^{15}N chemical shifts allowed determination of the four pK_a values of the His37 tetrad.[8,10] In virus-mimetic lipid bilayers, the His37 tetrad protonates with pK_a values of 7.6, 6.8, 4.9, and 4.2. When compared with pH-dependent proton currents, these pK_a values indicate that the +3 channels conduct the majority of the proton current at the physiological pH of the endosome.[8] A 1.65-Å X-ray crystal structure showed that the four histidines form an extensive hydrogen-bonding network with a cluster of water molecules,[11] suggesting proton delocalization. One helical turn away from His37, Trp41 is responsible for inward rectification of the channel.[12] Cation−π interaction between His37 and Trp41 was observed in resonance Raman spectra[13] and suggested by molecular dynamics (MD) simulations.[14] Recent solid-state NMR distance and dynamics data showed that at low pH Trp41 moved closer to His37 and underwent microsecond side chain reorientations.[15] The resulting periodic cation−π interactions with the cationic His37 may restrict proton release from His37, thus explaining the low proton flux compared to the water−His proton exchange rate.

The M2 proton channel is inhibited by the amantadine class of antiviral drugs, which blocks the N-terminal region of the

Received: April 25, 2013
Published: June 11, 2013

dx.doi.org/10.1021/ja4041412 | J. Am. Chem. Soc. 2013, 135, 9885−9897

channel pore near residue Ser31.[16−19] Bound at this site, amantadine (Figure 1) dehydrates the aqueous pore,[20] which

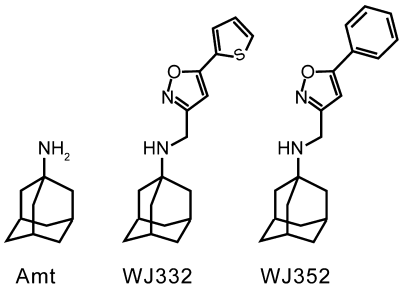

Figure 1. Chemical structures of adamantyl-based drugs against influenza M2 proton channels: amantadine (Amt) against the WT protein, and WJ332 and WJ352 against the S31N mutant.

prevents protonation of the His37 side chains,[8,21] in turn stopping conformational changes of the helix backbone and the imidazole rings that are important for proton conduction.[8] However, in the past decade, several amantadine-resistant TM mutations have become widespread in the M2 proteins of circulating flu viruses.[22] The most prevalent drug-resistant mutant, S31N, dominates in H1N1, H5N1, and H3N2 strains isolated from humans, birds, and swine.[23−25] The replacement of the hydroxyl group by the bulkier carboxamide at residue 31 not only abolished amantadine binding,[26,27] but also gave rise to a moderately better proton channel, with ∼20% higher single-channel conductance than the wild-type (WT) protein.[28]

To inhibit the S31N-M2 channel, Wang et al. recently designed a family of isoxazole compounds.[29] By functionalizing the heterocyclic isoxazole with amantadine and aryl substituents, they identified molecules that selectively inhibit S31N-M2 with a potency greater than that of amantadine against the WT channel. Solution NMR structures of the S31N M2(19−49) peptide in DPC micelles[29] bound with one such compound, 5-(thiophen-2-yl)-3-(*N*-adamantyl-methylamine)-1,2-isoxazole (WJ332), showed both similarities and major differences to the structure of amantadine-complexed WT peptide.[18] This drug is a derivative of amantadine, in which the basic amine group is linked to a biheteroaryl group via a methylene group (Figure 1), which retains the basicity of the amine. In the solution NMR structure of the S31N-WJ332 complex, the adamantane group is located in approximately the same region of the channel as amantadine in the WT, but it is flipped by 180° so that the pendant amino group projects upward toward the outside of the channel rather than downward toward His37, in contrast to the direction of amantadine and rimantadine in WT M2.[19] MD simulations based on the structure indicate that the N31 backbone carbonyl group helps solvate the ammonium group of WJ332 via water-mediated interactions, and the isoxazole group of the drug additionally interacts with N31.

Given the reversed direction of the isoxazole drug in micelle-bound S31N-M2, the predicted small energy difference between the amine-up and amine-down orientations, and the possibility of detergent micelles affecting drug binding, we wish to verify the binding mode of the isoxazole drug in phospholipid-bilayer-bound S31N-M2 using solid-state NMR spectroscopy. To facilitate isotopic labeling of the drug, we chose WJ352, a potent analogue of WJ332 in which the terminal thiophene is replaced by a phenyl group (Figure 1). Solid-state NMR also allows us to answer important questions about the charge state of the tetramer recognized by the drug. Amantadine binds with greater affinity to the neutral form of the channel than to the low-pH forms.[30] The neutral form may be stabilized by amantadine in part because the charged ammonium destabilizes the cationic form of His37 and in part because the neutral form of the channel has a conformation that is more complementary to the shape of the drug.[18] However, the ammonium group of the reverse oriented isoxazole is more distant from His37, so it was not clear whether the isoxazole would bind exclusively to the neutral state of the channel, or whether it might also associate with partially charged channels. Finally, studies in phospholipid bilayers allow us to examine the conformational and proton exchange dynamics of S31N-M2, since the mutant appeared more mobile than the WT peptide in detergent micelles.[26,29]

Using magic-angle-spinning (MAS) solid-state NMR spectroscopy, we have now measured the effects of WJ352 on the chemical shifts of key TM residues in S31N and on the proton exchange dynamics of His37. Chemical shift perturbation and drug−peptide distance measurements show that the adamantyl group is located between N31 and G34 while the phenyl tail points to the N-terminus. ^{15}N and ^{13}C chemical shifts of His37 show that S31N-M2 undergoes faster proton exchange with water than the WT. This exchange causes rapid interconversion among three states of His, which is observed for the first time. Drug binding suppressed most of the chemical exchange, providing direct evidence of the mechanism of inhibition of this mutant proton channel.

MATERIALS AND METHODS

Isotopically Labeled Peptides and Drugs. Two peptide constructs were used in this study, one spanning residues 19−49 and the other spanning residues 22−46 of the S31N mutant of the Udorn strain of M2. The amino acid sequence of residues 19−49 is SNDSSDPLVVAANIIGILHLILWILDRLFFK. Three isotopically labeled peptides were synthesized by using an optimized protocol as described previously.[19] After cleavage from the resin, the crude peptide was precipitated in cold ether and purified via HPLC (Vydac, C4 column). The first peptide contained ^{13}C,^{15}N-labeled residues at G34, I35, H37, and L38 ($GIHL_{22-46,S31N}$). The second sample contained ^{13}C,^{15}N-labeled V27, A30, N31, I33, and G34 ($VANIG_{19-49,S31N}$). The third sample contained ^{13}C,^{15}N-labeled V28, G34, I35, H37, and L38 ($VGIHL_{19-49,S31N}$).

5-Phenyl-3-(*N*-adamantyl-methylamine)-1,2-isoxazole (WJ352) was synthesized using a modified procedure from that described previously[29] to incorporate deuterium labels. The synthesis protocol is provided in the Supporting Information. Two compounds were synthesized, one with deuterated benzene (d_5-WJ352) and the other with perdeuterated adamantane (d_{15}-WJ352) (Figure S1). The purified drugs were verified by ^{1}H solution NMR and electrospray ionization mass spectrometry to have the correct chemical structures.

Membrane Sample Preparation. The isotopically labeled peptides were reconstituted in two types of lipid membranes. The first membrane is 1,2-dimyristoyl-*sn*-glycero-3-phosphocholine (DMPC), and the second is a virus-mimetic lipid mixture (VM+) containing 1-palmitoyl-2-oleoyl-*sn*-glycero-3-phosphocholine (POPC), 1-palmitoyl-2-oleoyl-*sn*-glycero-3-phosphoethanolamine (POPE), egg sphingomyelin (SM), and cholesterol (Chol) at molar ratios of 25.6%:25.6%:25.6%:23%. DMPC vesicles were prepared by eight to ten freeze−thaw cycles. The VM+ lipids were first mixed and dissolved in chloroform/methanol 1:1 (v:v). The bulk of the organic solvents were removed with nitrogen gas, then the lipids were dissolved in cyclohexane and lyophilized overnight. The resulting homogeneous dry powder was suspended in buffer, vortexed, and subjected to eight freeze−thaw cycles to create uniform vesicles. The M2 peptide was solubilized in octyl-β-D-glucoside (OG) solution and mixed with the

dx.doi.org/10.1021/ja4041412 | J. Am. Chem. Soc. 2013, 135, 9885−9897

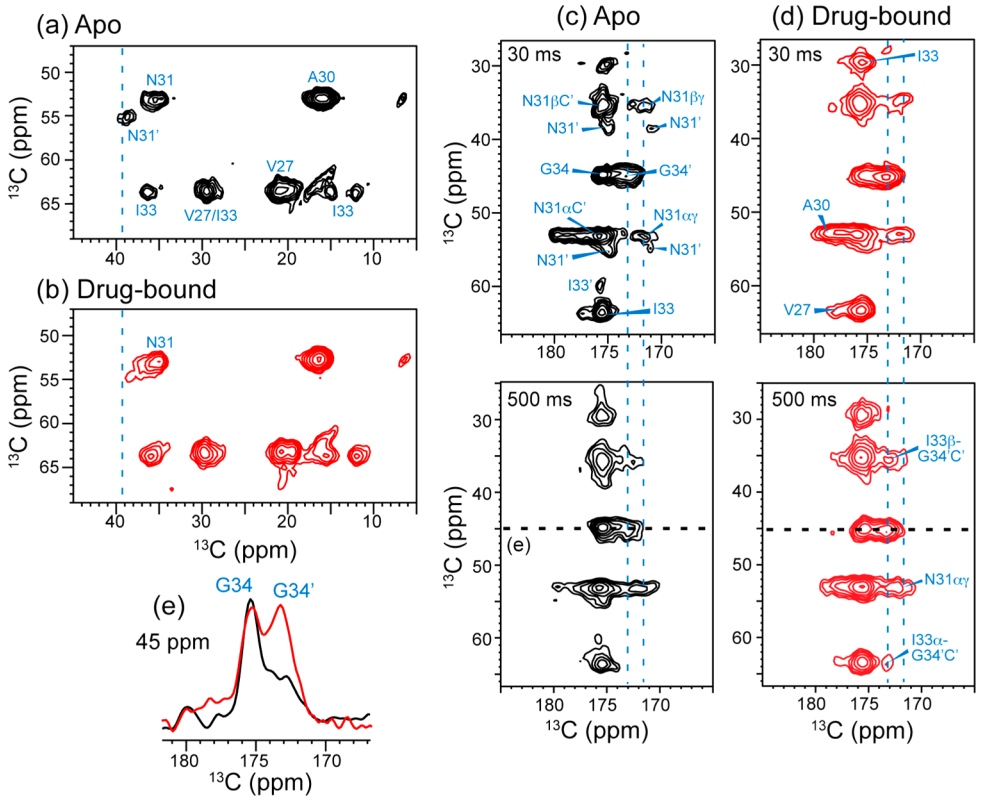

Figure 2. 2D $^{13}C-^{13}C$ correlation spectra of $VANIG_{19-49,S31N}$ in DMPC bilayers without and with WJ352 at pH 6.5. (a, b) Aliphatic region of the 30 ms spectra of the apo peptide (a) and drug-bound peptide (b). Drug binding changed the conformational equilibrium of the N31 Cα–Cβ peaks. (c, d) Carbonyl region of the 30 ms (top) and 500 ms (bottom) spectra of the (c) apo and (d) drug-bound peptide. N31, I33, and G34 exhibit two sets of chemical shifts. (e) The 45-ppm cross section of the apo (black) and drug-bound (red) peptide, showing the G34 Cα–CO cross peak. All spectra were measured at 243 K under 7 kHz MAS.

lipid vesicle solution. The peptide–lipid mixture was vortexed for 2 h, then dialyzed at room temperature against 1 L of buffer for 3 days with 6 buffer changes. The dialyzed proteoliposomes were spun down at 55 000 rpm at 5° C for 4 h to yield homogeneous membrane pellets, which were spun into 4 mm MAS rotors for solid-state NMR measurements. The peptide-to-lipid molar ratio was 1:15 for all the samples and the hydration level was 40–50% (by mass).

In total, nine membrane samples were used in this study. Three $GIHL_{22-46,S31N}$ samples were reconstituted into the DMPC membrane at pH 7.5 with a Tris buffer (10 mM Tris base, 1 mM EDTA, 0.1 mM NaN_3). The first sample contained no drug (apo), the second contained d_5-WJ352 at a drug:tetramer molar ratio of 1:1, and the third contained d_5-WJ352 at a drug:tetramer ratio of 8:1. Three $VANIG_{19-49,S31N}$ samples were reconstituted into DMPC bilayers at pH 6.5 with a phosphate buffer (10 mM NaH_2PO_4/Na_2HPO_4, 1 mM EDTA, 0.1 mM NaN_3). The first sample contained no drug, the second sample contained d_{15}-WJ352 at a drug:tetramer ratio of 1:1, and the third sample contained d_{15}-WJ352 at a drug:tetramer ratio of 10:1. Three $VGIHL_{19-49,S31N}$ samples were prepared in the VM+ membrane to investigate His37 structure and dynamics. Two of these samples were prepared at pH 5.4 with use of a citrate buffer (10 mM citric acid/sodium citrate, 1 mM EDTA, 0.1 mM NaN_3), one without drug and the other with protonated WJ352 at a drug:tetramer ratio of 10:1. The third sample was prepared at pH 7.5 with a phosphate buffer without drug.

For drug-bound samples, the desired aliquot of a stock ethanol solution containing the drug was dried and redissolved in 20–30 μL of ethanol. This concentrated solution was titrated into the membrane pellets from ultracentrifugation and mixed thoroughly to ensure homogeneous distribution of the drug. The membranes were then dried to remove ethanol and rehydrated before being spun into the MAS rotors for solid-state NMR measurements.

Solid-State NMR Experiments. All MAS NMR experiments were carried out on Bruker DSX-400 MHz (9.4 T) and AVANCE 600 MHz (14.1 T) spectrometers (Karlsruhe, Germany), using 4 mm triple resonance MAS probes tuned to $^1H/^{13}C/^{15}N$ and $^1H/^{13}C/^2H$ frequencies. Typical radiofrequency (rf) field strengths were 50–63 kHz for ^{13}C, 42 kHz for ^{15}N, 50 kHz for ^2H, and 62–83 kHz for ^1H. ^{13}C chemical shifts were referenced to the methylene signal of adamantane at 38.48 ppm on the tetramethylsilane scale and ^{15}N chemical shifts were referenced to the ^{15}N signal of *N*-acetylvaline at 122.0 ppm on the liquid ammonia scale. Sample temperature was controlled using a FTS Systems XR401 Air-Jet cooler, with an additional liquid nitrogen heat exchanger placed in series for temperatures below 240 K.

One-dimensional (1D) ^{13}C and ^{15}N MAS spectra were recorded with a cross-polarization (CP) sequence under 7 kHz MAS. Spectra were measured at 308 K to detect conformational motion and proton exchange, and between 190 and 243 K to determine the rigid-limit conformation of the peptide and the protonation state and tautomeric structure of His37. 1D $^{13}C-^{13}C$ double-quantum (DQ) filtered spectra were measured at 200 K or 230 K under 7 kHz MAS using the SPC5 sequence[31] to suppress the natural abundance ^{13}C signals of lipids. $^{15}N-^{13}C$ dipolar filtered 1D ^{13}C spectra were measured at 7 kHz with use of a REDOR-based pulse sequence.[32] Two-dimensional (2D) $^{13}C-^{13}C$ ^1H-driven spin diffusion (PDSD) experiments were conducted under 7 kHz MAS with a 30 ms mixing time between 230 and 308 K. 2D $^{15}N-^{13}C$ correlation spectra were measured at 230 and 308 K under 10 kHz MAS for the $VGIHL_{19-49,S31N}$ samples, and at 243 K under 7 kHz MAS for the $VANIG_{19-49,S31N}$ samples. A $^{13}C-^{15}N$ REDOR period of 0.8 ms was used to obtain one-bond $^{15}N-^{13}C$ correlation peaks. Under 10 kHz MAS, the Cγ resonance of His37 was suppressed by rotational resonance with the directly bonded Cβ,[33] thus allowing the distinction between the Nδ1 and Nϵ2 signals in the 2D spectra.

dx.doi.org/10.1021/ja4041412 | J. Am. Chem. Soc. 2013, 135, 9885–9897

$^{13}C-^{2}H$ REDOR experiments for determining peptide−drug spatial contact were conducted with and without $^{13}C-^{13}C$ DQ filtering.[18,34,35] The former was used to remove the lipid natural abundance signals in case of severe overlap with the peptide ^{13}C signals. Both types of REDOR experiments include a selective ^{13}C Gaussian pulse to suppress $^{13}C-^{13}C$ J coupling.[36] The DQ filtered REDOR experiments were carried out on the $VANIG_{19-49,S31N}$ sample under 5 kHz MAS, while the regular selective REDOR experiments were carried out on the $GIHL_{22-46,S31N}$ sample under 4.5 kHz MAS. In all REDOR experiments, a control (S_0) experiment without ^{2}H pulses and a dephasing (S) experiment with ^{2}H pulses were conducted back to back. ^{13}C sites close to the ^{2}H spins have lower intensities in the S spectrum than the S_0 spectrum. The ratio S/S_0 thus reflects $^{2}H-^{13}C$ distances: the shorter the distances, the lower the S/S_0 value. All REDOR spectra were measured at 243 K with 20 000−80 000 scans of signal averaging.

Solution NMR Experiments. Peptide and drug were added to deuterated dodecylphosphocholine (DPC) (Cambridge Isotope Laboratory) powder from their ethanol stocks at the desired molar ratios. Ethanol was removed by nitrogen purging, followed by overnight lyophilization. A phosphate buffer (10% D_2O, 50 mM sodium phosphate, pH 6.8) was added to the dried mixture to make a 2 mM (monomer) S31N M2(19−49) sample with 20 mM WJ332 or WJ352 in 100 mM deuterated DPC.

Two 2D ^{13}C-(^{1}H)-^{1}H NOESY spectra were measured on selectively labeled $VANIG_{19-49,S31N}$, using a Bruker 900 MHz Avance II spectrometer equipped with a cryogenic probe. The experiments were conducted at 313 K with a mixing time of 150 ms, $t_{1,max}$ of 7 ms, and $t_{2,max}$ of 71 ms, and 128 scans per t_1 slice. The ^{1}H carrier frequency was set to the water signal. The ^{1}H chemical shift was referenced to the residual water peak at 4.63 ppm relative to DSS while the ^{13}C chemical shift was referenced indirectly via the gyromagnetic ratio. The spectra were processed and analyzed using the NMRPipe program.[37] The first three time points of the indirect ^{13}C dimension were extended by linear prediction. Time domain data were multiplied by sine square bell window functions shifted by 90° and zero-filled once before Fourier transformation.

Calculation of Chemical Shift Perturbation. To examine drug-induced conformational change, we calculated the average chemical shift perturbation (CSP) of each residue between the apo and drug-bound states using the following empirical relation:[38]

$$\Delta\delta_{av} = \left\{\frac{1}{n}\left[\sum_{i=1}^{n-1}(\Delta\delta_{C,i})^2 + \left(\frac{\Delta\delta_N}{2.5}\right)^2\right]\right\}^{1/2}$$

where n is the total number of chemical shifts measured in each residue and $\Delta\delta$ is the individual-site's chemical shift difference between the apo and drug-bound states. We used chemical shifts obtained from the DMPC-bound membrane samples, with the exception of V28, which was only labeled in the $VGIHL_{19-49,S31N}$ sample bound to the VM+ membrane. For residues N31, I33, and G34, drug binding did not create new chemical shifts but changed the equilibrium between two sets of chemical shifts. We used the difference between these two sets of chemical shifts to represent drug perturbation of the conformation of these residues. For His37, a single set of backbone chemical shifts was observed for the apo peptide, and drug binding created a second set, so the average difference between these two sets of chemical shift was calculated. Only the Nα, CO, Cα, and Cβ chemical shifts were used in the His37 calculation, because imidazole chemical shifts are sensitive to chemical structure factors not directly related to conformational changes.

RESULTS

Drug-Induced Chemical Shift Changes of S31N-M2. We first investigated the effects of the isoxazole drug on S31N-M2 structure by analyzing the chemical shifts of the TM residues. Figures 2 and 3 show representative 2D $^{13}C-^{13}C$ and $^{15}N-^{13}C$ correlation spectra of DMPC-bound S31N-M2 at pH 6.5. Among the five labeled N-terminal residues (V27, A30, N31, I33, and G34), the isoxazole drug either selected one of the conformations or changed the equilibrium between multiple conformations. For example, N31 exhibits two sets of Cα and Cβ chemical shifts whereas G34 exhibits two CO chemical shifts. Drug binding largely removed the signals of the more α-helical chemical shifts of N31, retaining the smaller Cα and CO chemical shifts (Table S1). Similarly, the less α-helical (smaller) CO chemical shift of G34 is a minor component in the apo peptide but is equally populated as the more helical (larger) CO chemical shift in the drug-bound state (Figure 2e). The less helical G34 chemical shift also shows cross peaks with I33 at long ^{13}C spin diffusion mixing times (Figure 2c,d). For A30, conformational heterogeneity was less pronounced in the apo state, but drug binding also changed the Cα, Cβ, and CO chemical shifts to less helical values (Figure 3).

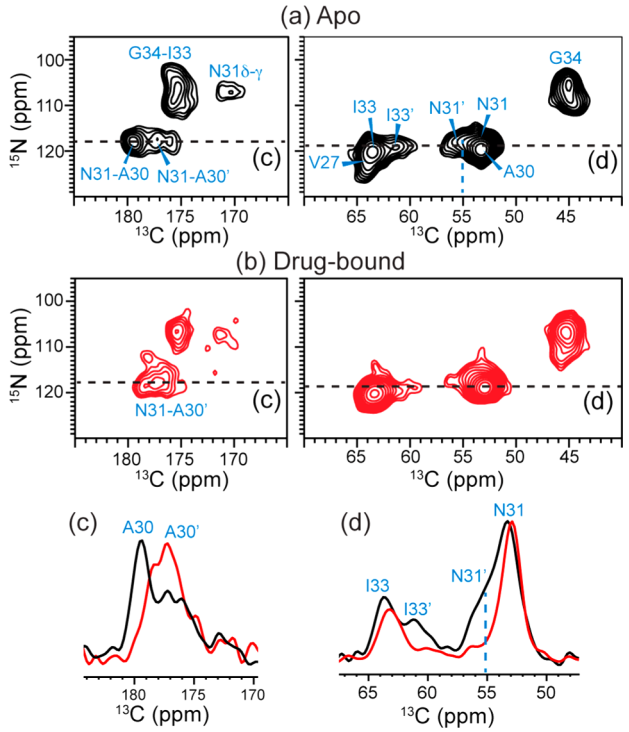

Figure 3. 2D $^{15}N-^{13}C$ correlation spectra of $VANIG_{19-49,S31N}$ in DMPC bilayers at pH 6.5: (a) without drug (black) and (b) with drug (red) at the 10:1 drug: tetramer ratio. (c) A30 CO cross section at the ^{15}N chemical shift of 117.6 ppm. Drug binding changed the intensity distribution of two A30 CO peaks. (d) I33 and N31 Cα cross section at 119.1 ppm ^{15}N chemical shift. Drug binding selected one of the two peaks of I33 and N31. The spectra were measured at 243 K under 7 kHz MAS.

Figure 4 shows the aliphatic region of the 2D ^{13}C PDSD spectra of $VGIHL_{19-49,S31N}$ in the VM+ membrane. Three samples with different pH and drug-binding states are compared. The chemical shifts show complex dependences on pH, drug binding, and temperature. At low temperature, the low-pH apo peptide exhibited a single set of Cα and Cβ chemical shifts for I35, H37, and L38, but upon drug binding and pH increase, these residues showed two sets of Cα and Cβ chemical shifts, indicating two distinct backbone conformations. Drug binding at low pH gave rise to the same two chemical shifts as those of the high-pH apo peptide, indicating that drug binding created the same conformational distribution as the closed state of the channel. The presence of two

dx.doi.org/10.1021/ja4041412 | J. Am. Chem. Soc. 2013, 135, 9885−9897

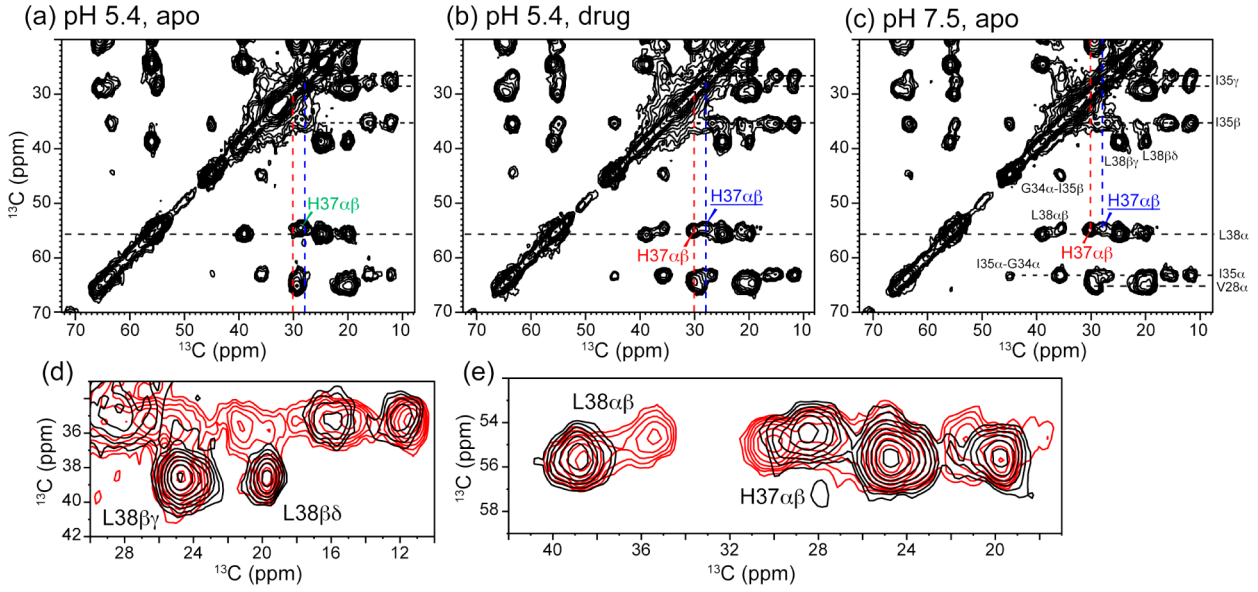

Figure 4. Aliphatic region of the 2D $^{13}C-^{13}C$ correlation spectra of VM+ membrane bound $VGIHL_{19-49,S31N}$. The spectra were measured at 243 K under 7 kHz MAS: (a) apo peptide at pH 5.4; (b) drug-bound peptide at pH 5.4; and (c) apo peptide at pH 7.5. The signals of τ, π, and cationic His37 are annotated in red, blue underline, and green, respectively. (d) Amplified L38 and I35 side chain region of the apo (black) and drug-bound (red) spectra at low pH. (e) Amplified H37 and L38 $C\alpha-C\beta$ region of the apo and drug-bound spectra at low pH. The low-pH drug-bound spectrum resembles the high-pH spectrum, indicating that WJ352 shifts the backbone conformation of S31N to that of the closed state.

backbone conformations of H37 in the drug-bound state is qualitatively reproduced in the DMPC membrane (not shown). Thus, the conformation of the functionally essential His37 is largely dictated by pH and drug binding and is not sensitive to the membrane environment.

I35 and L38 exhibit a single set of side chain chemical shifts in the low-pH apo peptide at low temperature, but at high temperature, both side chains show two sets of chemical shifts (Figure S2), which are similar to those of the high-pH and drug-bound samples. These observations indicate that the energetic balance between the two side chain conformations of these interfacial residues changes between the open state and the closed or inhibited state of the channel. The minor conformation is less stable in the open state and thus not populated at low temperature, but it is stabilized in the closed and inhibited states.

To compare the magnitudes of the chemical shift changes of the various residues by the drug, we calculated the CSP. Figure 5 shows that N31 has the largest chemical shift perturbation, followed by H37 and G34. This trend is very similar to the effect of amantadine on the WT peptide, where S31 was the site of maximum chemical shift perturbation, followed by G34 and V28.[39] H37 was not included in the WT chemical shift perturbation study.

Interestingly, while N31 exhibited the largest chemical shift perturbation, the Asn side chain $C\gamma$ chemical shift is relatively unaffected by the drug. This is seen in the 2D spectra in Figures 2c,d and 3, and further verified in $^{15}N-^{13}C$ filtered 1D ^{13}C spectra measured between 190 and 270 K (Figure S3). Below 240 K, the $C\gamma$ intensities are consistently 7−10% of the full spectral intensity, indicating full detection of this signal and ruling out the possibility of an invisible dynamic population. The absence of $C\gamma$ chemical shift change indicates that the average N31 rotameric conformation is little affected by the drug. However, at 270 K, the $C\gamma$ intensity in the drug-bound sample appears lower than in the apo sample (Figure S3),

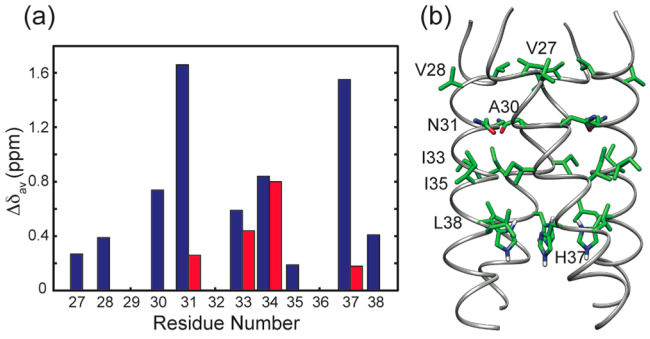

Figure 5. (a) Residue-specific average chemical shift change in S31N M2TM induced by the drug WJ352. Residues with a single set of chemical shifts in both the apo and drug-bound states have a single blue bar for the average CSP, while residues with two sets of chemical shifts in the apo state but only one set in the drug-bound state have two CSP values. (b) Solution NMR structure of S31N M2TM (PDB: 2LY0), showing the positions of most residues whose CSPs were measured.

suggesting the onset of rotameric exchange, whose detail will require further experiments to elucidate.

WJ352 Binding Site in the S31N-M2 Channel. The ability of WJ352 and its derivatives to inhibit the S31N-M2 channel[29] is somewhat surprising given the larger size of the isoxazoles compared to amantadine and rimantadine and the more constricted channel due to the replacement of Ser by Asn. To investigate how exactly the bulky isoxazole fits into the S31N channel, we selectively deuterated WJ352 either at the adamantane head (d_{15}) or at the phenyl tail (d_5). Using the versatile REDOR experiment, we measured the location and orientation of deuterated WJ352 bound to ^{13}C-labeled S31N-M2.

For d_5-WJ352 complexed $GIHL_{22-46,S31N}$, we did not observe $^{13}C-^{2}H$ REDOR intensity differences between the control (S_0) and dephased (S) spectra at drug:tetramer ratios of either 1:1

dx.doi.org/10.1021/ja4041412 | J. Am. Chem. Soc. 2013, 135, 9885−9897

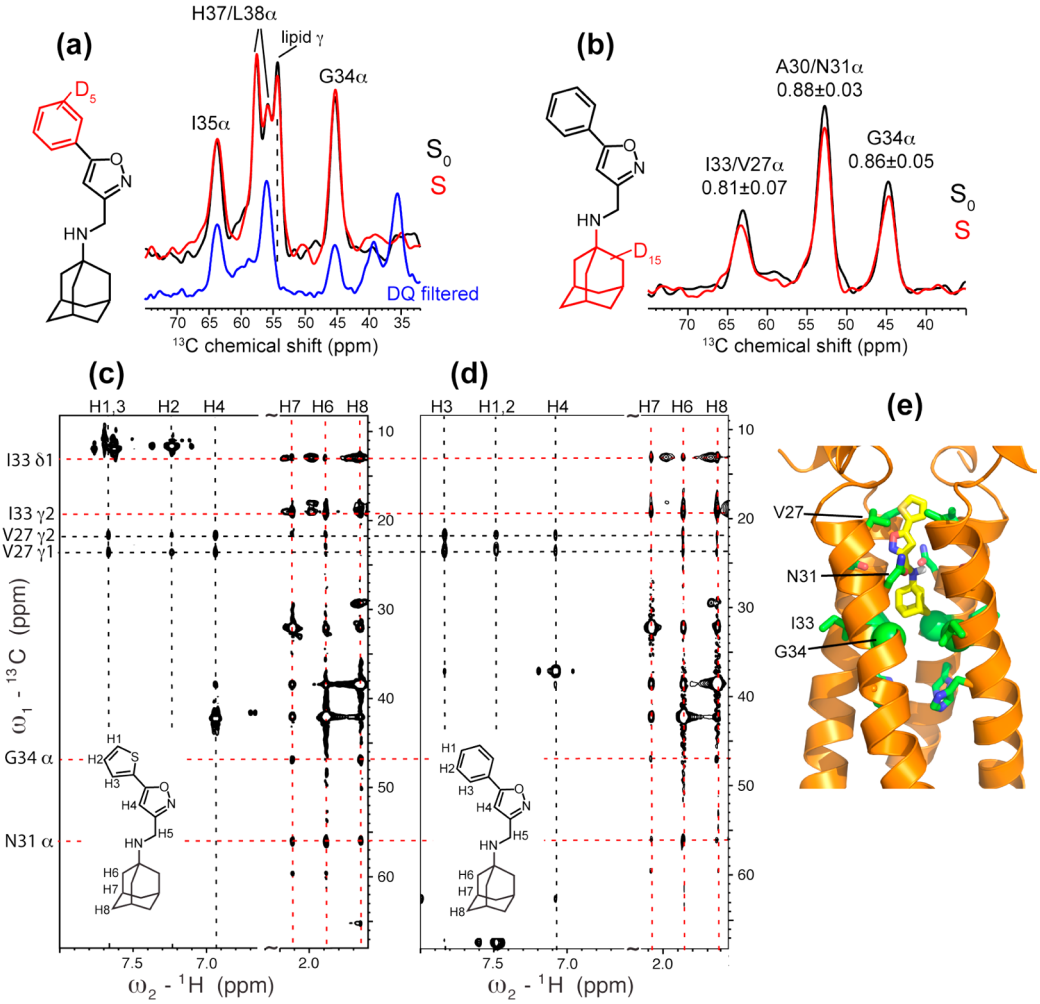

Figure 6. Binding site and orientation of WJ352 in S31N bound to DMPC bilayers (a, b) and DPC micelles (c, d). (a) $^{13}C-^{2}H$ REDOR S_0 (black) and S (red) spectra of d_5-WJ352 complexed $GIHL_{22-46,S31N}$ in DMPC bilayers. The mixing time was 14.2 ms and the drug:tetramer ratio was 8:1. The deuterated phenyl group did not dephase any peptide ^{13}C signals, especially G34. The REDOR spectra were measured without DQ filtering, thus showing a lipid headgroup Cγ peak at 54 ppm. This is verified by the absence of the peak in a ^{13}C DQ filtered spectrum (blue). (b) $^{13}C-^{2}H$ DQ filtered REDOR spectra of d_{15}-WJ352 bound $VANIG_{19-49,S31N}$ in DMPC bilayers. The mixing time was 9.6 ms and the drug:tetramer ratio was 1:1. The deuterated adamantane dephased multiple ^{13}C signals. (c, d) 2D ^{13}C-(^{1}H)-^{1}H NOESY (150 ms) spectra of $VANIG_{19-49,S31N}$ in DPC micelles with bound WJ332 (c) or with bound WJ352 (d). Drug–peptide cross peaks are observed and consistent with the amine-up orientation. (e) Solution NMR structure of S31N-M2 with bound WJ332 (PDB: 2LY0).[29]

or 8:1. In particular, the well-resolved G34 Cα signal had no intensity change (Figure 6a), indicating that the phenyl tail is far from this segment. Under excess drug, the lipid headgroup Cγ showed moderate intensity reduction in the S spectrum, indicating that excess WJ352 partitions to the membrane–water interface, analogous to amantadine and rimantadine.[40,41] In comparison, d_{15}-WJ352 complexed $VANIG_{19-49,S31N}$ showed clearly lower S intensities than the S_0 intensities for most labeled sites both at the stoichiometric drug concentration (Figure 6b) and under excess drug (data not shown). At a REDOR mixing time of 9.6 ms, the I33/V27 Cα peak exhibits an S/S_0 value of 0.81 ± 0.07, the A30/N31 Cα peak has an S/S_0 value of 0.88 ± 0.03, while G34 Cα has S/S_0 = 0.86 ± 0.05. These REDOR spectra were measured under ^{13}C DQ filtering to suppress the lipid ^{13}C signals, thus the low sensitivity prohibits the use of longer mixing times to quantify the distances. Although the V27 and I33 Cα peaks overlap, I33 likely contributes to the majority of the measured REDOR dephasing at 64 ppm because of the proximity of I33 to G34, whose Cα signal also shows significant REDOR dephasing. Taken together, these spectra indicate that WJ352 binds to the channel lumen with the adamantane head spanning the segment from A30 to G34, while the phenyl tail is directed toward the N-terminus. Solution-state $^{13}C-^{1}H$ NOESY spectra of $VANIG_{19-49,S31N}$ in DPC micelles confirmed this result: the adamantane H6, H7, and H8 protons show clear cross peaks with I33 side chains while the phenyl H1–H4 protons exhibit cross peaks with V27 side chains (Figure 6c,d). Thus, the solution and solid-state NMR spectra indicate that in both lipid bilayers and DPC micelles, the isoxazole drug binds to the S31N channel pore with the amine pointing to the exterior (Figure 6e).

Effects of Isoxazole Drug on His37 Structure and Dynamics. To investigate how S31N conducts protons and how drug binding interferes with this conduction, we measured the His37 ^{15}N and ^{13}C chemical shifts, which are highly sensitive to the protonation state and tautomeric structure of the His side chain.[42−45] Figures 7 and 9 show 1D ^{15}N and ^{13}C spectra of $VGIHL_{19-49,S31N}$ at high temperature (308 K) where dynamic processes are active and at low temperature where

dx.doi.org/10.1021/ja4041412 | J. Am. Chem. Soc. 2013, 135, 9885−9897

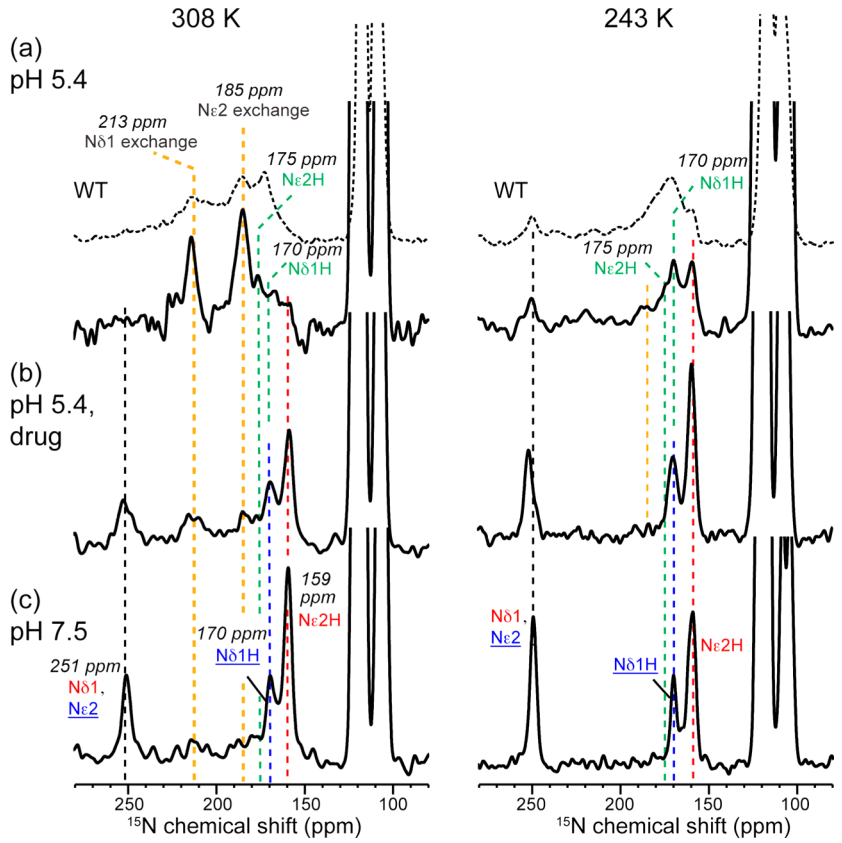

Figure 7. 1D ^{15}N CP-MAS spectra of His37 in VM+ membrane bound VGIHL$_{19-49,S31N}$ at 308 (left) and 243 K (right). The spectra were scaled to show roughly equal integrated intensities for the imidazole nitrogens: (a) apo peptide at pH 5.4; (b) drug-bound peptide at pH 5.4; and (c) apo peptide at pH 7.5. Assignments shown here and in subsequent figures are annotated in red for the τ tautomer, blue underline for the π tautomer, and green for cationic His. For comparison, the pH 5.2 spectra of WT His37 are shown (dotted line) above the S31N spectra in part a. At low pH and high temperature, S31N-M2 exhibited sharp ^{15}N exchange peaks. WJ352 binding largely suppressed these peaks.

rigid-limit chemical shifts allow quantification of the various species of histidine present under a certain condition. The ^{15}N and ^{13}C chemical shifts were assigned based on the 2D spectra in Figure 8 and Figure S4 and by comparison with the WT data.[6,8]

For the high-pH apo peptide, the ^{15}N spectra (Figure 7c) show the Nε2H peak of the τ tautomer (159 ppm) and the Nδ1H peak of the π tautomer (170 ppm), similar to WT M2TM.[6] The unprotonated ^{15}N peak at 251 ppm has high intensity, indicating that neutral histidines dominate at this pH. Since the multiple protonated nitrogens are not well resolved between neutral and cationic His, the presence of cationic His is better ascertained from the ^{13}C spectra (Figure 9c). The Cδ2 chemical shift is an excellent indicator of the τ tautomer, π tautomer, and cationic His.[46] At pH 7.5 all three species were detected: the τ tautomer (Cδ2 at 114 ppm) dominates, followed by the π tautomer (Cδ2 at 124 ppm), while a weak cationic Cδ2 peak at 117 ppm is also detected in the DQ filtered and ^{15}N−^{13}C filtered ^{13}C spectra. Thus, cationic His indeed exists at a low percentage at this neutral pH, similar to the WT channel.[8]

In the low-pH apo peptide, the low-temperature ^{15}N spectrum shows a strong and broad peak at ~170 ppm (Figure 7a). The large width of this peak distinguishes it from the π tautomer Nδ1H peak at high pH and identifies it as cationic Nδ1H, as verified by 2D correlation spectra (Figure 8a and Figure S4a). The unprotonated ^{15}N signal (251 ppm) is weak, furthur indicating that the percentage of neutral His is much lower than at pH 7.5. Increasing the temperature to 308 K dramatically changed the ^{15}N spectra: two dominant signals appear at intermediate ^{15}N chemical shifts of 213 and 185 ppm, indicating fast interconversion of various His species. Both peaks were also observed in the WT ^{15}N spectra, but with much large line widths.[8] In addition to these two peaks, a significant intensity band between 160 and 180 ppm was also detected and constitutes about 30% of the total aromatic intensity.

Drug binding to the low-pH channel largely reverted the ^{15}N spectra to those of the high-pH apo state (Figure 7b): at low temperature, the broad cationic ^{15}N signals between 170 and 180 ppm sharpened to become the signature of the π tautomer Nδ1H peak, while the 251-ppm peak greatly increased its intensity. The spectrum resembles the high-pH spectrum at low temperature. Increasing the temperature gave rise to residual exchange intensities at 213 and 185 ppm, but the spectrum remains dominated (~70%) by the sharp signals at the frequencies of neutral His. Thus, isoxazole binding at low pH converted most of the cationic His's to the neutral, non-conducting conformation.

To elucidate the origin of the 213- and 185-ppm peaks, we measured 2D ^{15}N−^{13}C correlation spectra (Figure 8), supplemented with 2D ^{13}C−^{13}C correlation spectra (Figure S4). The 185-ppm ^{15}N peak is correlated to two ^{13}C signals (134 and 118 ppm) while the 213-ppm peak is correlated only to a 134-ppm peak (Figure 8a). These 2D ^{15}N−^{13}C correlation spectra were measured under 10 kHz MAS, near the rotational-resonance condition[33] between Cβ and Cγ of His37, which

dx.doi.org/10.1021/ja4041412 | J. Am. Chem. Soc. 2013, 135, 9885−9897

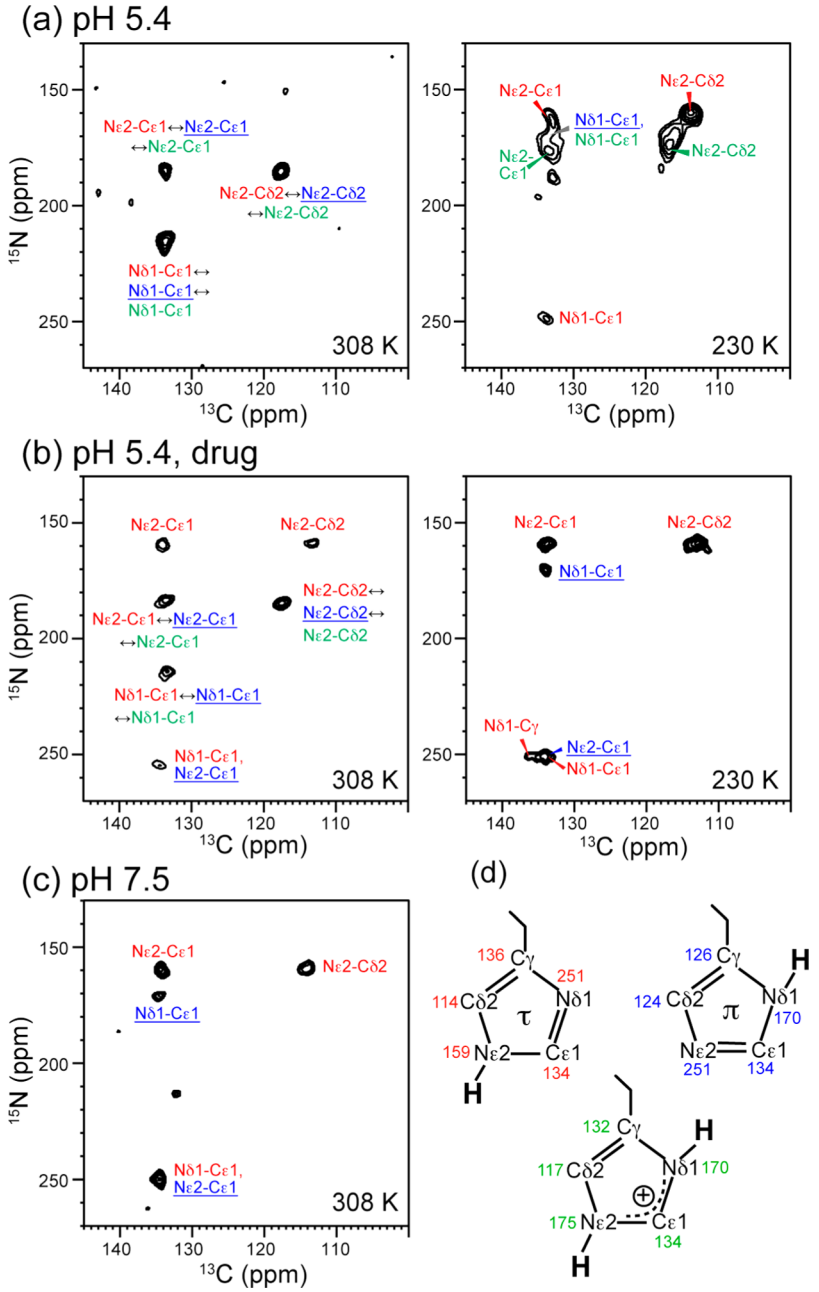

Figure 8. 2D ^{15}N–^{13}C correlation spectra of VM+ bound VGIHL$_{19-49,S31N}$ at 308 and 230 K under 10 kHz MAS: (a) apo peptide at pH 5.4; (b) drug-bound peptide at pH 5.4; and (c) apo peptide at pH 7.5. The Cγ signal was not detected due to rotational resonance with Cβ, thus allowing the distinction between Nδ1 and Nε2 signals. (d) Imidazole chemical shifts for the τ tautomer, π tautomer, and cationic His.

broadened the Cγ signal. As a result, Nδ1 has only one correlation peak (to Cε1) while Nε2 has two correlation signals (to Cε1 and Cδ2). Thus, the 213-ppm signal must be assigned to Nδ1 while the 185-ppm peak must be assigned to Nε2. Similarly, at high pH (Figure 8c), the 170-ppm ^{15}N peak can be assigned to Nδ1 while the 159-ppm peak was confirmed to result from Nε2. The 2D ^{15}N–^{13}C correlation spectrum of the drug-bound sample (Figure 8b) confirms the 1D observation that the sample is a mixture of a small fraction of unbound channels with exchange peaks and bound channels in which His37 adopts the high-pH apo structure.

The low-temperature 1D ^{13}C spectra (Figure 9) allow us to quantify the concentrations of the three His species in each sample based on the distinct Cδ2 chemical shifts.[46] At pH 7.5, the concentration ratios are 65%:25%:10% (±5%) for τ:π:cationic His, indicating the predominance of neutral His. For the apo pH 5.4 sample, the ratios are 36%:12%:52% (±5%), indicating that half of the His are cationic. The drug-bound sample showed concentration ratios of 60%:28%:12% (±10%) for τ:π:cationic His, quantitatively indicating that isoxazole converted most His to the neutral form at this low pH.

DISCUSSION

Isoxazole Binding Site and the Effects of Drug on S31N-M2 Conformation. The observed ^{13}C and ^{15}N chemical shifts indicate that the isoxazole drug perturbed the conformation of S31N in a similar fashion as amantadine to

dx.doi.org/10.1021/ja4041412 | J. Am. Chem. Soc. 2013, 135, 9885–9897

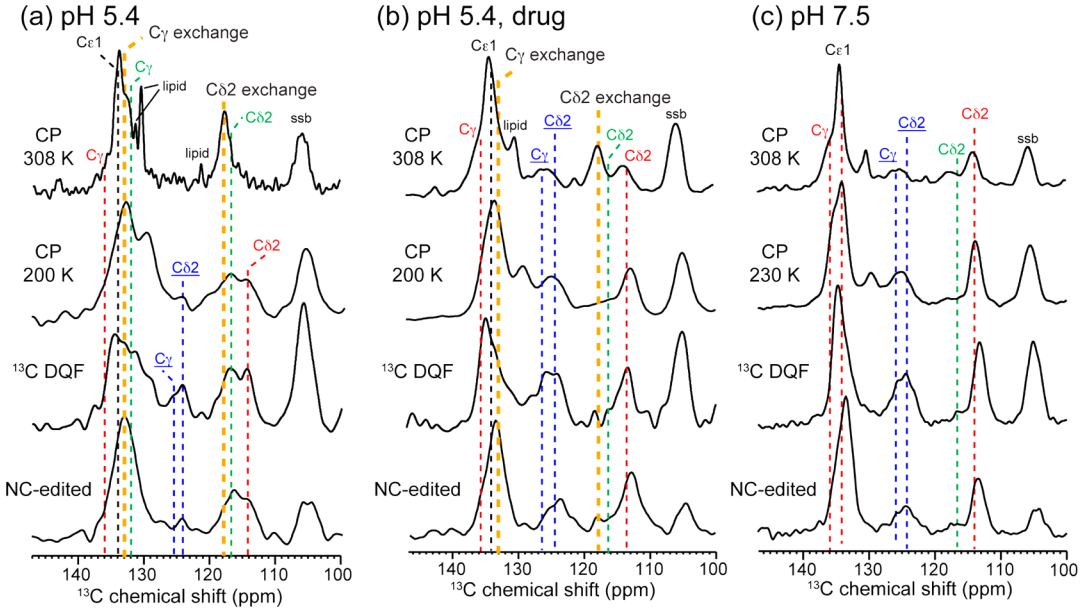

Figure 9. Aromatic region of the 1D ^{13}C MAS spectra of His37 in VM+ bound $VGIHL_{19-49,S31N}$. From top to bottom are the 308 K ^{13}C CP-MAS spectra, the low-temperature CP-MAS (200 or 230 K) spectra, the low-temperature $^{13}C-^{13}C$ DQ filtered (DQF) spectra, and the low-temperature $^{15}N-^{13}C$ filtered spectra: (a) apo peptide at pH 5.4; (b) drug-bound peptide at pH 5.4; and (c) apo peptide at pH 7.5. Spinning sidebands are denoted as ssb. All spectra were measured under 7 kHz MAS.

wild-type M2TM. Most importantly, the drug significantly changed the Cα and Cβ chemical shifts of residue 31, thus achieving the design purpose of targeting this amantadine-resistant mutation site. Both amantadine and isoxazole perturbed the chemical shifts of G34, whose conformation is known to be sensitive to the environment.[39,47,48] However, a major difference exists in the way that the two drugs are oriented in the pore. While amantadine and rimantadine are oriented with the polar amine pointing down to H37,[19] the biaryl isoxazoles are flipped by 180° and point the polar amine up to the exterior, as evidenced by $^{13}C-^{2}H$ REDOR data and NOE cross peaks (Figure 6). This opposite orientation suggests that both amantadine and isoxazole drugs are significantly stabilized by hydrophobic interactions of the adamantane with the peptide, mainly at the segment between N31 and G34 (Figure 6e).[18] In addition to the hydrophobic interaction, MD simulations show the presence of multiple hydrogen bonds between the amine and the Asn side chains and between the isoxazole nitrogen and the Asn side chains, which should further stabilize the amine-up orientation.[29]

Isoxazole binding shifted the conformational equilibrium of various residues, selecting one of two conformations at N31, I33, and G34 while creating two conformations at H37. The nature of the two conformations in apo S31N-M2 is not yet fully understood. A longer construct of the protein, S31N M2(18−60), was also reported to show peak doubling, which was found for most residues.[27] The current data on the TM construct suggest that one possible cause of the two conformations is tautomerism of His37, since the two His37 Cβ chemical shifts are individually correlated to the τ and π resonances (Figure S4). This hypothesis is supported by the observation that the two C$\alpha-$Cβ peaks of Leu38 have similar intensity ratios as the His37 C$\alpha-$Cβ peak intensity ratios in the high-pH sample (Figure 4b,c).

Interestingly, while the drug selected one of the two backbone conformations of N31, the carboxamide Cγ chemical shift is largely unaffected by the drug at low temperature (Figure S3), indicating that the average rotameric conformation of N31 is unperturbed by the drug. On the other hand, the N31 side chain chemical shifts of DMPC-bound S31N M2(19−49) measured here differ significantly from the N31 chemical shifts of S31N M2(18−60) bound to the diphytanoylphosphocholine membrane:[27] the Cγ and Nδ chemical shifts are about 173 (DSS scale) and 106 ppm in the current study (Table S1) but 175−178 and 113−115 ppm, respectively, in the previous study. These differences indicate that the rotameric structures of N31 may be sensitive to the lipid membrane and/or the peptide construct length.

An increasing number of membrane proteins have been found to adopt multiple conformations under different conditions and undergo slow exchange among these conformations.[49] For example, the structures of phospholamban,[40] the G-protein coupled receptor β_2-adrenoreceptor,[35] wild-type influenza M2 transmembrane peptide,[47,50] and viral fusion peptides[51−53] are all significantly influenced by the membrane composition, and other factors such as temperature[54] and pH[55] can also modulate membrane protein structure. Such conformational plasticity is usually associated with function, such as ion channel opening, closing, and inactivation;[41,56,57] enzyme catalysis;[58] and protein−protein interactions.[40] The fact that drug binding to S31N-M2TM did not simply cause a conformational change but selected a subset of conformations that pre-existed in the apo peptide[59] suggests that the energy landscape of the M2 transmembrane domain, even in the lipid bilayer instead of detergent micelles,[60] is rough, and this roughness may be relevant for the multiple functions of M2, including proton conduction,[2] membrane scission,[61] and virus assembly,[62] in addition to drug binding.[5]

Proton-Exchange Dynamics of His37 in S31N-M2. The conformation and dynamics of His37 in S31N reveal the proton conduction mechanism of the M2 channels. Similar to the WT channel, S31N shows His37 exchange dynamics at low pH, as manifested by the 213- and 185-ppm ^{15}N chemical shifts and the associated ^{13}C exchange peaks.[8] Also similar to the WT

dx.doi.org/10.1021/ja4041412 | J. Am. Chem. Soc. 2013, 135, 9885−9897

channel, these exchange peaks are highly sensitive to temperature (Figure 7a), indicating significant energy barriers, which support the assignment of these peaks to His−water proton transfer[5,7] rather than strong His−His hydrogen bonding,[14] which would be essentially barrier-less.[63] The rate of this His−water proton transfer is discernibly faster for S31N than for WT M2, as evidenced by the narrower line widths of the ^{15}N exchange peaks. This difference is qualitatively consistent with the higher proton conductance of S31N than the WT channel.[28] On the other hand, the conductance difference is only about 20%, while the His−water proton transfer rate difference appears much larger. We recently calculated an exchange rate of $\sim 10^5$ s^{-1} for WT M2[8] based on the exchange line widths. This rate is already more than 2 orders of magnitude larger than the proton flux per second.[9] We attribute the smaller proton flux partly to the interaction of His37 with the gating residue, Trp41.[12] Recent solid-state NMR data of WT M2TM indicate that at low pH, Trp41 moves closer to His37 by ∼2 Å and undergoes larger-amplitude side chain reorientation.[15] The resulting periodic cation−π interactions with His37 should reduce the number of protons released from His37 to water. Similar Trp41−His37 interactions should be present in S31N as well, which would reduce the number of protons transported into the virion.

Further insight into the mechanism of His-mediated proton transfer is obtained by determining the nature and populations of the molecular species that give rise to the ^{15}N exchange peaks. The similar line widths of the two ^{15}N exchange peaks (Figures 7a and 8a) suggest that they originate from the same exchange process. Since protonated nitrogens have ^{15}N chemical shifts below ∼185 ppm, the 213-ppm ^{15}N exchange peak is only possible when unprotonated nitrogens constitute roughly 50% of the interconverting His species.[8] Since both τ and π tautomers contain unprotonated nitrogens, all three His species can in principle participate in exchange. Using the rigid-limit ^{15}N chemical shifts (Table 1), we solve for three simultaneous linear equations,

$$213\ \text{ppm} = 251\ \text{ppm}\cdot f_\tau + 170\ \text{ppm}\cdot f_\pi + 170\ \text{ppm}\cdot f_+$$

$$185\ \text{ppm} = 159\ \text{ppm}\cdot f_\tau + 251\ \text{ppm}\cdot f_\pi + 175\ \text{ppm}\cdot f_+$$

$$1 = f_\tau + f_\pi + f_+$$

which gives molar fractions of f_τ = 53%, f_π = 24%, and f_+ = 23% for τ, π, and cationic His.

Table 1. ^{15}N and ^{13}C Chemical Shifts (ppm) of Individual His37 in S31N-M2 Bound to the Virus−Mimetic Membrane

site	τ tautomer	π tautomer	cation	obsd τ:π:cation 53:24:23 exchange
Cα	55.4	54.8	54.8	55.1[a]
Cβ	30.1	27.9	28.4	29.2
Cγ	136	126	132	133
Nδ1	251	170	170	213
Cε1	134	134	134	134[a]
Nε2	159	251	175	185
Cδ2	114	124	117	118

[a]These are predicted exchange-averaged chemical shifts that are not resolved from unexchange peaks.

This three-site exchange model is confirmd by the high-temperature ^{13}C spectrum of the apo peptide (Figure 9a), where the main Cδ2 signal at 118 ppm can be distinguished from the cationic Cδ2 peak (117 ppm) as well as the neutral Cδ2 peaks (124 ppm for π and 114 ppm for τ) at low temperature. This 118-ppm peak is consistent with the weighted average of the three rigid-limit Cδ2 chemical shifts, but inconsistent with any two-site exchange models such as τ−cationic or τ−π exchange. For example, a τ−cationic exchange model that agrees with the 213-ppm ^{15}N peak would require a 1:1 ratio, which would lead to an average Cδ2 chemical shift of less than 117 ppm, in contradiction with the measured Cδ2 chemical shift. The three-site exchange with the above ratios predicts an average Cγ chemical shift of 133 ppm, which is also detected in the high-temperature spectrum. Cε1 is insensitive to exchange because all three states of His have the same rigid-limit Cε1 chemical shift of 134 ppm. Taken together, the high-temperature ^{13}C spectra and the clear identification of the 185-ppm ^{15}N peak as an exchange peak revise our previous understanding of the interconverting His species during His−water proton transfer, by including the π tautomer in the exchange.

The τ:π:cationic ratio of 53%:24%:23% obtained from the exchange-averaged ^{15}N chemical shifts is noteworthy, because the cationic fraction is much lower than expected, and lower than the low-temperature ^{13}C spectra derived cationic His concentration of ∼52% (Figure 9a). This apparent discrepancy is resolved by the fact that the observed exchange peaks mainly result from tetramers with low charge states of +1 and +2, where only one or two His residues are cationic. Higher-charged, +3 and +4, tetramers, which are also populated at pH 5.4 based on the measured pK_a values of the WT channel,[8] do not contribute to these specific ^{15}N exchange peaks because they give average ^{15}N chemical shifts in the 160−190 ppm range, which cannot be easily distinguished from nonexchange protonated nitrogen signals. Indeed, the 160−180 ppm band in the low-pH high-temperature ^{15}N spectrum (Figure 7a) constitutes ∼30% of the total aromatic intensity, and is consistent with the presence of exchange signals from higher charged tetramers. In other words, exchange within low-charged tetramers is more detectable due to a high population of unprotonated nitrogens, which shifts the average ^{15}N frequencies downfield, away from the protonated ^{15}N signals. If we combine the 30% cationic His intensity from the 160−180 band with the cationic His fraction from the exchange peaks, which is ∼23% of the remaining 70% aromatic intensity (∼70% × 23% = 16%), then we indeed obtain a higher cationic fraction of close to 50%, in good agrement with the low-temperature ^{13}C intensities.

In addition to charge-conserved interconversion of the four histidines within a tetramer, the charge state of a tetramer can also change due to net His−water proton transfer, which may be considered as intertetramer exchange. More definitive information about the second process will require further experiments. What is clear from the current data is that high pH suppresses both intratetramer fast exchange and any possible intertetramer exchange, even though a small fraction (10%) of cationic His remains.

The fast τ−π−cationic His interconversion at low pH refines our model of the His37-mediated proton transfer in M2 channels (Figure 10).[6] In this model, in addition to proton acquisition by a neutral His to convert to the cationic state and proton release by the cation to a neutral His, τ and π tautomers

dx.doi.org/10.1021/ja4041412 | J. Am. Chem. Soc. 2013, 135, 9885−9897

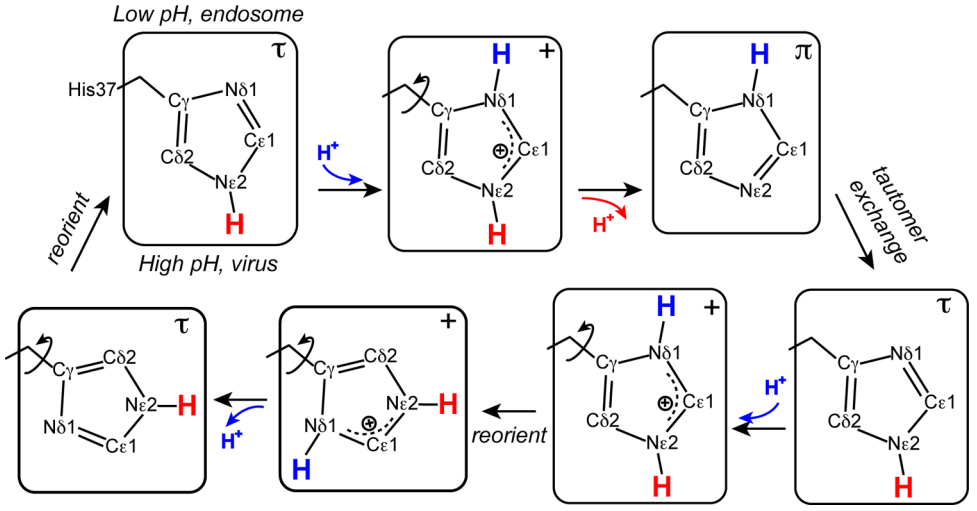

Figure 10. Proposed mechanism of His37-water proton exchange for S31N and WT M2 channels. His37 residues undergo rapid interconversion among τ, π, and cationic states during proton transfer with water. Ring reorientations facilitate this proton shuttling by pointing the unprotonated nitrogen toward the low-pH exterior.

can exchange rapidly by coupled release of a proton on one nitrogen (e.g., Nδ1) and acquisition of a proton on the other nitrogen (e.g., Nε2). Such prototropic tautomerism of heterocycles has been studied extensively,[64,65] and is known to involve much lower energy barriers when it is mediated by solvent molecules instead of proceeding purely by an intramolecular mechanism. Thus, His37 interaction with water molecules on both sides of the ring is most likely required for this tautomerism to occur. Indeed, exchange-averaged ^{1}H chemical shifts associated with the His37 nitrogens were recently measured for WT M2 and were shown to be close to the water ^{1}H chemical shift at high temperature,[7] indicating that the proton-transfer partner of all three His species is water. Ring motion remains important in the model, to orient the imidazolium with water molecules to achieve proton transfer.

Although the model in Figure 10 depicts only the dynamic transformations of a single His residue, in reality the process should reflect the ensemble average of all His's in each tetramer, since protons relayed from one His can be transferred via water to a neighboring His. This model is applicable to both S31N and WT channels, based on the fundamental similarity of the observed exchange frequencies.

Effects of the Isoxazole Drug on His37−Water Proton Exchange. Binding of the isoxazole drug, although only as deep as G34, largely suppressed the His−water proton exchange, and changed the His37 chemical shifts to a form similar to the high-pH closed state. These are fully consistent with the observed Cα and Cβ chemical shifts, which also indicate a reversion of the peptide conformation to that of the closed state. Thus, isoxazole binding dehydrates the S31N channel, and interrupts the water wire that leads to His37,[5] which inhibits proton shuttling by His37.

Although we did not directly measure the pK_a values of the His37 tetrad in S31N-M2, the similar pH-dependence of the ^{15}N spectra between the S31N and WT peptides[8] suggests similar thermodynamic parameters for protonation and deprotonation. This implies that the pH 5.4 apo S31N in the VM+ membrane should contain significant amounts of +2 and +3 tetramers. We showed recently that the +3 channel has the highest specific conductance for the WT peptide, and in this state the imidazole undergoes ring reorientation and proton exchange.[6,8] Any effective drug must therefore inhibit the +3 charged channels. In general, the drug affinity to the channel is pH dependent: for example, titration of WJ352 to DPC-bound S31N showed an optimal pH of 6.8 for drug binding,[29] which is close to the third pK_a of S31N-M2 in DPC micelles. But the effective pK_a values are sensitive to the membrane environment: a more dynamic membrane causes higher pK_a values. In the chain-saturated virus−mimetic membrane the WT M2 has a third pK_a of 4.9. The more dynamic, unsaturated, VM+ membrane[66] used here is expected to increase the His pK_a values moderately, so the third pK_a should shift to between pH 5 and 6. Thus, S31N in the VM+ membranes at pH 5.4 may have a similar charge distribution as S31N in DPC micelles at pH 6.8: both should be dominated by +2 and +3 channels, and both are inhibited by the isoxazole drugs based on the NMR spectra. Therefore, both micelle and bilayer data suggest that the isoxazole drugs significantly inhibit the activated channel at acidic pH. This may result from the reduced sensitivity of the amine-up drug to the charge state of His37 and from the bulky size of the drug, whose larger contact area with the peptide makes it less sensitive to small shape differences between the low-pH and high-pH channel pores.

■ CONCLUSION

In conclusion, we found that the isoxazole drug WJ352 perturbed the conformational equilibrium of S31N-M2, shifting the TM segment to a less ideal helical conformation. N31 exhibits the largest chemical shift perturbation, similar to S31 of the WT protein in complex with amantadine. In the low-pH S31N channel, the four His37 residues of the tetramer undergo proton transfer with water more rapidly than the WT channel, causing fast interconversion among τ, π, and cationic His. This exchange is more easily detected for tetramers with low charge states but is also present for the high-charge states. Drug binding at low pH suppressed most of the chemical exchange process, reverting the His37 residues to a similar charge distribution as that of the high-pH closed state. The conformation of other TM residues also reverts to the closed state structure. Therefore, the isoxazole drug, while bound more than one helical turn away from His37, potently arrests

dx.doi.org/10.1021/ja4041412 | J. Am. Chem. Soc. 2013, 135, 9885−9897

the atomic processes that shuttle protons in this proton channel.

■ ASSOCIATED CONTENT

Supporting Information

Additional NMR spectra, tables, and experimental methods. This material is available free of charge via the Internet at http://pubs.acs.org.

■ AUTHOR INFORMATION

Corresponding Author

mhong@iastate.edu

Notes

The authors declare no competing financial interest.

■ ACKNOWLEDGMENTS

This work is funded by NIH grants GM088204 to M.H. and AI074571 to W.F.D.

■ REFERENCES

(1) Lamb, R. A.; Holsinger, K. J.; Pinto, L. H. In *Cellular Receptors of Animal Viruses*; Wemmer, E., Ed.; Cold Spring Harbor Lab Press: Plainview, NY, 1994; pp 303−321.
(2) Pinto, L. H.; Lamb, R. A. *J. Biol. Chem.* **2006**, *281*, 8997−9000.
(3) Sugrue, R. J.; Bahadur, G.; Zambon, M. C.; Hall-Smith, M.; Douglas, A. R.; Hay, A. J. *EMBO J.* **1990**, *9*, 3469−3476.
(4) Wang, C.; Lamb, R. A.; Pinto, L. H. *Biophys. J.* **1995**, *69*, 1363−1371.
(5) Hong, M.; Degrado, W. F. *Protein Sci.* **2012**, *21*, 1620−1633.
(6) Hu, F.; Luo, W.; Hong, M. *Science* **2010**, *330*, 505−508.
(7) Hong, M.; Fritzsching, K. J.; Williams, J. K. *J. Am. Chem. Soc.* **2012**, *134*, 14753−14755.
(8) Hu, F.; Schmidt-Rohr, K.; Hong, M. *J. Am. Chem. Soc.* **2012**, *134*, 3703−3713.
(9) Lin, T. I.; Schroeder, C. *J. Virol.* **2001**, *75*, 3647−3656.
(10) Hu, J.; Fu, R.; Nishimura, K.; Zhang, L.; Zhou, H. X.; Busath, D. D.; Vijayvergiya, V.; Cross, T. A. *Proc. Natl. Acad. Sci. U.S.A.* **2006**, *103*, 6865−6870.
(11) Acharya, A.; Carnevale, V.; Fiorin, G.; Levine, B. G.; Polishchuk, A.; Balannick, V.; Samish, I.; Lamb, R. A.; Pinto, L. H.; DeGrado, W. F.; Klein, M. L. *Proc. Natl. Acad. Sci. U.S.A.* **2010**, *107*, 15075−15080.
(12) Tang, Y.; Zaitseva, F.; Lamb, R. A.; Pinto, L. H. *J. Biol. Chem.* **2002**, *277*, 39880−39886.
(13) Okada, A.; Miura, T.; Takeuchi, H. *Biochemistry* **2001**, *40*, 6053−6060.
(14) Sharma, M.; Yi, M.; Dong, H.; Qin, H.; Peterson, E.; Busath, D.; Zhou, H. X.; Cross, T. A. *Science* **2010**, *330*, 509−512.
(15) Williams, J. K.; Zhang, Y.; Schmidt-Rohr, K.; Hong, M. *Biophys. J.* **2013**, *104*, 1698−1708.
(16) Hay, A. J.; Wolstenholme, A. J.; Skehel, J. J.; Smith, M. H. *EMBO J.* **1985**, *4*, 3021−3024.
(17) Stouffer, A. L.; Acharya, R.; Salom, D.; Levine, A. S.; Di Costanzo, L.; Soto, C. S.; Tereshko, V.; Nanda, V.; Stayrook, S.; DeGrado, W. F. *Nature* **2008**, *451*, 596−599.
(18) Cady, S. D.; Schmidt-Rohr, K.; Wang, J.; Soto, C. S.; DeGrado, W. F.; Hong, M. *Nature* **2010**, *463*, 689−692.
(19) Cady, S. D.; Wang, J.; Wu, Y.; DeGrado, W. F.; Hong, M. *J. Am. Chem. Soc.* **2011**, *133*, 4274−4284.
(20) Luo, W.; Hong, M. *J. Am. Chem. Soc.* **2010**, *132*, 2378−2384.
(21) Hu, J.; Riqiang, F.; Cross, T. A. *Biophys. J.* **2007**, *93*, 276−283.
(22) Bright, R. A.; Shay, D. K.; Shu, B.; Cox, N. J.; Klimov, A. I. *JAMA* **2006**, *295*, 891−894.
(23) Hurt, A. C.; Selleck, P.; Komadina, N.; Shaw, R.; Brown, L.; Barr, I. G. *Antiviral Res.* **2007**, *73*, 228−231.
(24) Zaraket, H.; Saito, R.; Suzuki, Y.; Suzuki, Y.; Caperig-Dapat, I.; Dapat, C.; Shabana, I. I.; Baranovich, T.; Suzuki, H. *Antiviral Ther.* **2010**, *15*, 307−319.
(25) Simonsen, L.; Viboud, C.; Grenfell, B. T.; Dushoff, J.; Jennings, L.; Smit, M.; Macken, C.; Hata, M.; Gog, J.; Miller, M. A.; Holmes, E. C. *Mol. Biol. Evol.* **2007**, *24*, 1811−1820.
(26) Pielak, R. M.; Schnell, J. R.; Chou, J. J. *Proc. Natl. Acad. Sci. U.S.A.* **2009**, *106*, 7379−7384.
(27) Andreas, L. B.; Eddy, M. T.; Chou, J. J.; Griffin, R. G. *J. Am. Chem. Soc.* **2012**, *134*, 7215−7218.
(28) Balannik, V.; Carnevale, V.; Fiorin, G.; Levine, B. G.; Lamb, R. A.; Klein, M. L.; Degrado, W. F.; Pinto, L. H. *Biochemistry* **2010**, *49*, 696−708.
(29) Wang, J.; Wu, Y.; Ma, C.; Fiorin, G.; Wang, J.; Pinto, L. H.; Lamb, R. A.; Klein, M. L.; Degrado, W. F. *Proc. Natl. Acad. Sci. U.S.A.* **2013**, *110*, 1315−1320.
(30) Wang, C.; Takeuchi, K.; Pinto, L. H.; Lamb, R. A. *J. Virol.* **1993**, *67*, 5585−5594.
(31) Hohwy, M.; Jakobsen, H. J.; Eden, M.; Levitt, M. H.; Nielsen, N. C. *J. Chem. Phys.* **1998**, *108*, 2686−2694.
(32) Hong, M.; Griffin, R. G. *J. Am. Chem. Soc.* **1998**, *120*, 7113−7114.
(33) Raleigh, D. P.; Levitt, M. H.; Griffin, R. G. *Chem. Phys. Lett.* **1988**, *146*, 71−76.
(34) Su, Y.; Doherty, T.; Waring, A. J.; Ruchala, P.; Hong, M. *Biochemistry* **2009**, *48*, 4587−4595.
(35) Chung, K. Y.; Kim, T. H.; Manglik, A.; Alvares, R.; Kobilka, B. K.; Prosser, R. S. *J. Biol. Chem.* **2012**, *287*, 36305−36311.
(36) Jaroniec, C. P.; Tounge, B. A.; Herzfeld, J.; Griffin, R. G. *J. Am. Chem. Soc.* **2001**, *123*, 3507−3519.
(37) Delaglio, F.; Grzesiek, S.; Vuister, G. W.; Zhu, G.; Pfeifer, J.; Bax, A. *J. Biomol. NMR* **1995**, *6*, 277−293.
(38) Foster, M. P.; Wuttke, D. S.; Clemens, K. R.; Jahnke, W.; Radhakrishnan, I.; Tennant, L.; Reymond, M.; Chung, J.; Wright, P. E. *J. Biomol. NMR* **1998**, *12*, 51−71.
(39) Cady, S. D.; Mishanina, T. V.; Hong, M. *J. Mol. Biol.* **2009**, *385*, 1127−1141.
(40) Gustavsson, M.; Traaseth, N. J.; Veglia, G. *Biochim. Biophys. Acta* **2012**, *1818*, 146−153.
(41) Shenkarev, Z. O.; Paramonov, A. S.; Lyukmanova, E. N.; Shingarova, L. N.; Yakimov, S. A.; Dubinnyi, M. A.; Chupin, V. V.; Kirpichnikov, M. P.; Blommers, M. J.; Arseniev, A. S. *J. Am. Chem. Soc.* **2010**, *132*, 5630−5637.
(42) Munowitz, M.; Bachovchin, W. W.; Herzfeld, J.; Dobson, C. M.; Griffin, R. G. *J. Am. Chem. Soc.* **1982**, *104*, 1192−1196.
(43) Li, S.; Hong, M. *J. Am. Chem. Soc.* **2011**, *133*, 1534−1544.
(44) Henry, B.; Tekely, P.; Delpuech, J. J. *J. Am. Chem. Soc.* **2002**, *124*, 2025−2034.
(45) Bachovchin, W. W. *Magn. Reson. Chem.* **2001**, *39*, S199−S213.
(46) Vila, J. A.; Arnautova, Y. A.; Vorobjev, Y.; Scheraga, H. A. *Proc. Natl. Acad. Sci. U.S.A.* **2011**, *108*, 5602−5607.
(47) Hu, F.; Luo, W.; Cady, S. D.; Hong, M. *Biochim. Biophys. Acta* **2011**, *1808*, 415−423.
(48) Hu, J.; Asbury, T.; Achuthan, S.; Li, C.; Bertram, R.; Quine, J. R.; Fu, R.; Cross, T. A. *Biophys. J.* **2007**, *92*, 4335−4343.
(49) Cross, T. A.; Sharma, M.; Yi, M.; Zhou, H. X. *Trends Biochem. Sci.* **2011**, *36*, 117−125.
(50) Li, C.; Qin, H.; Gao, F. P.; Cross, T. A. *Biochim. Biophys. Acta* **2007**, *1768*, 3162−3170.
(51) Bodner, M. L.; Gabrys, C. M.; Struppe, J. O.; Weliky, D. P. *J. Chem. Phys.* **2008**, *128*, 052319.
(52) Yao, H.; Hong, M. *J. Mol. Biol.* **2013**, *425*, 563−576.
(53) Lai, A. L.; Moorthy, A. E.; Li, Y.; Tamm, L. K. *J. Mol. Biol.* **2012**, *418*, 3−15.
(54) Su, Y.; Mani, R.; Doherty, T.; Waring, A. J.; Hong, M. *J. Mol. Biol.* **2008**, *381*, 1133−1144.
(55) Ader, C.; Schneider, R.; Seidel, K.; Etzkorn, M.; Becker, S.; Baldus, M. *J. Am. Chem. Soc.* **2009**, *131*, 170−176.

(56) Takeuchi, K.; Takahashi, H.; Kawano, S.; Shimada, I. *J. Biol. Chem.* **2007**, *282*, 15179−15186.
(57) Bhate, M. P.; Wylie, B. J.; Tian, L.; McDermott, A. E. *J. Mol. Biol.* **2010**, *401*, 155−166.
(58) Hwang, P. M.; Bishop, R. E.; Kay, L. E. *Proc. Natl. Acad. Sci. U.S.A.* **2004**, *101*, 9618−9623.
(59) Cady, S. D.; Hong, M. *Proc. Natl. Acad. Sci. U.S.A.* **2008**, *105*, 1483−1488.
(60) Stouffer, A. L.; Ma, C.; Cristian, L.; Ohigashi, Y.; Lamb, R. A.; Lear, J. D.; Pinto, L. H.; DeGrado, W. F. *Structure* **2008**, 1067−1076.
(61) Rossman, J. S.; Jing, X.; Leser, G. P.; Lamb, R. A. *Cell* **2010**, *142*, 902−913.
(62) Rossman, J. S.; Lamb, R. A. *Virology* **2011**, *411*, 229−236.
(63) Song, X. J.; McDermott, A. E. *Magn. Reson. Chem.* **2001**, *39*, S37−S43.
(64) Elguero, J.; Katritzky, A. R.; Denisko, O. V. *Adv. Heterocycl. Chem.* **2000**, *76*, 1−84.
(65) Minkin, V. I.; Garnovskii, A. D.; Elguero, J.; Katritzky, A. R.; Denisko, O. V. *Adv. Heterocycl. Chem.* **2000**, *76*, 157−323.
(66) Cady, S. D.; Wang, T.; Hong, M. *J. Am. Chem. Soc.* **2011**, *133*, 11572−11579.